ISSN No:-2456-2165 https://doi.org/10.38124/ijisrt/26sep054

Hybrid Nanofluid Flow Over a Riga Plate Surrounded by a Variable Porous Medium with Thermal Radiation

Abdul Qayyum[1*]; Abdul Wahab[2]

[1]Centre for Advanced Studies in Pure and Applied Mathematics, Bahauddin Zakariya University, Multan, 60800, Pakistan
[2]University of Southern Punjab, Multan, Pakistan

Corresponding Author: Abdul Qayyum[*]

Publication Date: 2026/09/10

Abstract: The present study investigates the boundary-layer flow and heat transfer characteristics of a hybrid nanofluid over a Riga plate embedded in a variable porous medium, taking into account the combined influence of thermal radiation. The Riga plate, an electromagnetic actuator composed of a spanwise arrangement of permanent magnets and alternating electrodes mounted on a flat surface, generates a wall-parallel Lorentz force that decays exponentially with distance from the plate, thereby offering an effective and non-mechanical means of controlling boundary layer flow without the need for direct fluid contact with moving parts. The working fluid considered is a hybrid nanofluid formed by dispersing two distinct nanoparticle species, typically a metallic and a metal-oxide nanoparticle, within a common base fluid, a combination known to enhance thermal conductivity beyond that achievable with a conventional single-nanoparticle suspension. The governing partial differential equations describing conservation of mass, momentum, and energy, incorporating the Riga plate electromagnetic body force term, a variable porous-medium permeability, and the Rosseland approximation for thermal radiation, are transformed into a system of coupled nonlinear ordinary differential equations via an appropriate similarity transformation. The resulting boundary-value problem is solved numerically using the shooting technique in conjunction with the fourth-order Runge–Kutta integration scheme and validated against previously published results for limiting cases. The influence of pertinent physical parameters, including the modified Hartmann number, porosity parameter, radiation parameter, and nanoparticle volume fraction, on the velocity and temperature profiles, as well as the skin friction coefficient and local Nusselt number, is examined in detail and presented in graphical and tabular form. The findings indicate that increasing the modified Hartmann number enhances fluid velocity near the plate, whereas increasing porosity and radiation parameters exert a retarding effect on the flow and a promoting effect on the thermal boundary layer thickness, respectively. The hybrid nanofluid is found to provide superior heat transfer performance compared to a conventional nanofluid under otherwise identical conditions, confirming its suitability for advanced thermal management applications.

Keywords: *Hybrid Nanofluid; Riga Plate; Variable Porous Medium; Thermal Radiation; Boundary Layer Flow; Electromagnetohydrodynamic.*

How to Cite: Abdul Qayyum; Abdul Wahab (2026) Hybrid Nanofluid Flow Over a Riga Plate Surrounded by a Variable Porous Medium with Thermal Radiation. *International Journal of Innovative Science and Research Technology*, 11(9), 66-75. https://doi.org/10.38124/ijisrt/26sep054

I. INTRODUCTION

The study of boundary layer flow over stretching or flat surfaces continues to attract significant research attention owing to its wide-ranging relevance to numerous industrial and engineering processes, including polymer extrusion, wire drawing, glass fiber production, and the cooling of electronic and metallurgical components. Within this broad field, the introduction of the Riga plate concept by Gailitis and Lielausis has provided researchers with a novel means of controlling boundary layer behavior through electromagnetic actuation rather than conventional mechanical or thermal means. A Riga plate consists of a spanwise arrangement of alternating electrodes and permanent magnets mounted flush with a flat surface, which together generate a wall-parallel Lorentz force within an electrically conducting fluid. This force decays exponentially with distance from the plate surface [1], [2], [3]. It has been shown to effectively suppress boundary layer separation and delay transition to turbulence, making the Riga plate configuration of considerable interest for applications in marine propulsion, submarine hull design, and flow control over aerodynamic surfaces.

ISSN No:-2456-2165 https://doi.org/10.38124/ijisrt/26sep054

In parallel with developments in electromagnetic flow control, the field of nanofluid research has matured considerably since the pioneering work of Choi, who first demonstrated that the dispersion of nanometer-sized solid particles within a conventional base fluid such as water, ethylene glycol, or engine oil could substantially enhance the thermal conductivity of the resulting suspension relative to the base fluid alone[4], [5]. This enhancement in thermal conductivity translates directly into improved convective heat transfer performance, motivating extensive subsequent research into nanofluid applications across heat exchangers, solar collectors, electronic cooling systems, and biomedical devices. More recently, the concept of the hybrid nanofluid has emerged as a natural extension of conventional single-particle nanofluids, involving the simultaneous dispersion of two or more distinct nanoparticle species, typically combining a metallic nanoparticle possessing very high thermal conductivity, such as copper or silver, with a metal-oxide nanoparticle offering favorable chemical stability, such as alumina or titania. Numerous experimental and theoretical studies have demonstrated that such hybrid combinations can achieve thermal conductivity enhancements exceeding those obtained with either nanoparticle type alone, while simultaneously mitigating practical drawbacks, such as sedimentation and increased viscosity, associated with high concentrations of a single nanoparticle species [6].

A further dimension of complexity relevant to many practical heat transfer applications arises from the presence of a porous medium surrounding the flow domain, as encountered in geothermal energy extraction, packed-bed reactors, and insulation systems. Unlike an idealized porous medium of constant permeability, many real porous materials exhibit spatially variable permeability arising from non-uniform packing, particle-size distributions, or manufacturing variability [7], [8]. This variable-porosity behavior has been shown to influence boundary-layer development meaningfully and must therefore be incorporated into realistic flow models. Additionally, in high-temperature applications such as nuclear reactor cooling, solar energy systems, and combustion processes, thermal radiation contributes significantly to overall heat transfer and cannot be neglected without introducing substantial modeling errors[9], [10]. The Rosseland diffusion approximation is commonly employed to incorporate radiative heat flux into the energy equation in a computationally tractable manner, particularly for optically thick media.

Despite the maturity of research on Riga plate flow control, hybrid nanofluid heat transfer enhancement, variable porous medium effects, and thermal radiation, comparatively limited attention has been directed toward their combined and simultaneous consideration within a single unified boundary-layer flow model [11], [12]. Such a combined analysis is of considerable practical relevance to emerging applications, including advanced marine thermal management systems, electromagnetically controlled microfluidic heat exchangers, and porous thermal insulation systems operating under radiative heating conditions. Motivated by this gap in the existing literature, the present study develops and numerically solves a comprehensive boundary layer model describing hybrid nanofluid flow over a Riga plate embedded within a variable porous medium under the influence of thermal radiation, to characterize the combined influence of these effects on the resulting velocity and temperature fields, as well as on the practically important skin friction coefficient and local Nusselt number [13], [14].

The remainder of this article is organized as follows. Section 2 presents the mathematical formulation of the problem, including the governing partial differential equations, the hybrid nanofluid thermophysical property models, and the similarity transformation employed to reduce the governing equations to a system of ordinary differential equations. Section 3 describes the numerical solution methodology and validation procedure. Section 4 presents and discusses the results obtained, supported by graphical and tabular data. Section 5 concludes the article with a summary of key findings and suggestions for future research directions.

II. MATHEMATICAL FORMULATION

➢ *Physical Model and Governing Equations*

Consider steady, two-dimensional, incompressible, laminar boundary layer flow of an electrically conducting hybrid nanofluid over a horizontal Riga plate coinciding with the x-axis, with the y-axis oriented normal to the plate surface [15], [16]. The plate is assumed to induce fluid motion through stretching with a velocity proportional to the streamwise coordinate, while simultaneously generating an electromagnetic body force in the streamwise direction owing to the arrangement of electrodes and permanent magnets characteristic of the Riga plate configuration. The surrounding medium is treated as a variable-porosity porous medium whose permeability varies with the streamwise coordinate, and the fluid is assumed to be optically thick, allowing the Rosseland approximation to model the radiative heat flux contribution in the thermal energy equation[17], [18]. Viscous dissipation and Joule heating are neglected in the present formulation for simplicity, consistent with common practice in comparable studies within this field.

Under the boundary-layer approximations, the governing equations for the conservation of mass, momentum, and energy for the hybrid nanofluid flow may be written as follows[19], [20], [21]. The continuity equation is given by

$$\frac{\partial u}{\partial x} + \frac{\partial v}{\partial y} = 0 \tag{1}$$

The momentum equation, incorporating the Riga plate electromagnetic body force term and the variable porous medium drag term, is given by

$$u\frac{\partial u}{\partial x} + v\frac{\partial u}{\partial y} = \frac{\mu_{hnf}}{\rho_{hnf}}\frac{\partial^2 u}{\partial y^2} + \frac{\pi j_0 M_0}{8\rho_{hnf}}\exp\left(-\frac{\pi y}{a}\right) - \frac{\mu_{hnf}}{\rho_{hnf}K(x)}u \tag{2}$$

The energy equation [22], incorporating the radiative heat flux contribution, is given by

ISSN No:-2456-2165 https://doi.org/10.38124/ijisrt/26sep054

$$u\frac{\partial T}{\partial x}+v\frac{\partial T}{\partial y}=\frac{k_{hnf}}{(\rho c_p)_{hnf}}\frac{\partial^2 T}{\partial y^2}-\frac{1}{(\rho c_p)_{hnf}}\frac{\partial q_r}{\partial y} \quad (3)$$

Where the radiative heat flux [23], following the Rosseland approximation, is expressed as

$$q_r=-\frac{4\sigma^*}{3k^*}\frac{\partial T^4}{\partial y} \quad (4)$$

With σ^* denoting the Stefan–Boltzmann constant and k^* the mean absorption coefficient. Expanding T^4 using a Taylor series [24], [25] about the ambient temperature T_∞ and retaining only the linear term, as is standard practice for this class of problem, yields the linearized form $T^4 \approx 4T_\infty^3 T - 3T_\infty^4$, which is subsequently substituted into the energy equation.

The associated boundary conditions describing the stretching Riga plate surface and the ambient free stream conditions are given by

$$u=U_w(x)=cx,\ v=0,\ T=T_w \text{ at } y=0 \quad (5)$$

$$u\to 0,\ T\to T_\infty \text{ as } y\to\infty$$

Where c is a positive constant characterizing the stretching rate of the plate, and T_w and T_∞ denote the wall and ambient temperatures, respectively [26].

➢ *Hybrid Nanofluid Thermophysical Properties*

The thermophysical properties of the hybrid nanofluid, formed by dispersing two distinct nanoparticle types within a common base fluid, are modeled using established mixture relations widely adopted in the hybrid nanofluid literature. The effective density of the hybrid nanofluid is given by

$$\rho_{hnf}=(1-\phi_2)\left[(1-\phi_1)\rho_f+\phi_1\rho_{s1}\right]+\phi_2\rho_{s2} \quad (6)$$

Where ϕ_1 and ϕ_2 denote the volume fractions of the first and second nanoparticle species, respectively, and ρ_f, ρ_{s1}, and ρ_{s2} denote the densities of the base fluid and the two nanoparticle materials [27], [28]. The effective dynamic viscosity is estimated using the Brinkman model, extended to the hybrid case as

$$\mu_{hnf}=\frac{\mu_f}{(1-\phi_1)^{2.5}(1-\phi_2)^{2.5}} \quad (7)$$

The effective thermal conductivity of the hybrid nanofluid is obtained through sequential application of the Maxwell model, first computing the effective thermal conductivity of a nanofluid containing only the first nanoparticle species [29], [30], and subsequently treating this nanofluid as the base fluid for the introduction of the second nanoparticle species, according to.

$$\frac{k_{hnf}}{k_{bf}}=\frac{k_{s2}+2k_{bf}-2\phi_2(k_{bf}-k_{s2})}{k_{s2}+2k_{bf}+\phi_2(k_{bf}-k_{s2})} \quad (8)$$

Where k_{bf} denotes the thermal conductivity of the nanofluid formed with the first nanoparticle species alone, computed through an analogous expression [31], [32]. Finally, the effective heat capacitance of the hybrid nanofluid is given by.

$$(\rho c_p)_{hnf}=(1-\phi_2)\left[(1-\phi_1)(\rho c_p)_f+\phi_1(\rho c_p)_{s1}\right]+\phi_2(\rho c_p)_{s2} \quad (9)$$

Representative thermophysical properties of the base fluid and nanoparticle materials commonly employed in hybrid nanofluid studies of this type are summarized in Table 1.

Table 1 Thermophysical Properties of Base Fluid and Nanoparticle Materials [33], [34].

Property	Water (base fluid)	Copper (Cu)	Alumina (Al_2O_3)
Density, ρ (kg/m³)	997.1	8933	3970
Specific heat, c_p (J/kg·K)	4179	385	765
Thermal conductivity, k (W/m·K)	0.613	400	40

➢ *Similarity Transformation*

To reduce the governing partial differential equations to a more tractable system of ordinary differential equations, the following similarity variables are introduced:

$$\eta=y\sqrt{\frac{c}{\nu_f}},\ \psi=\sqrt{c\nu_f}\,xf(\eta),\ \theta(\eta)=\frac{T-T_\infty}{T_w-T_\infty} \quad (10)$$

Where ψ denotes the stream function, defined in the usual manner such that $u=\partial\psi/\partial y$ and $v=-\partial\psi/\partial x$, thereby automatically satisfying the continuity equation [35], [36]. The variable porous medium permeability is assumed to take the form $K(x)=K_0(1+\epsilon x)^{-1}$, consistent with common practice for representing spatially varying porosity in boundary layer studies, where K_0 is a reference permeability and ϵ a small parameter characterizing the degree of permeability variation.

Substitution of the similarity variables into the governing momentum and energy equations yields the following coupled system of nonlinear ordinary differential equations:

$$\frac{A_2}{A_1}f'''+ff''-(f')^2+\frac{A_2}{A_1}Q\exp(-\gamma\eta)-\frac{A_2}{A_1}\lambda f'=0 \quad (11)$$

$$\frac{1}{Pr}\left(\frac{k_{hnf}/k_f}{A_3}+\frac{4}{3}\frac{Nr}{A_3}\right)\theta''+f\theta'=0 \quad (12)$$

Subject to the transformed boundary conditions

$$f(0)=0,\ f'(0)=1,\ \theta(0)=1$$

$$f'(\eta)\to 0,\ \theta(\eta)\to 0 \text{ as } \eta\to\infty$$

Where the coefficients $A_1, A_2,$ and A_3 represent the density, viscosity, and heat capacitance ratios of the hybrid

ISSN No:-2456-2165 https://doi.org/10.38124/ijisrt/26sep054

nanofluid relative to the base fluid, respectively, arising naturally from the substitution of the hybrid nanofluid property models presented in Section 2.2. In these equations, $Q = \pi j_0 M_0/(8a\rho_f c^2 x)$ denotes the modified Hartmann number characterizing the strength of the Riga plate electromagnetic actuation; γ is a dimensionless decay parameter associated with the exponential decay of the Lorentz force; $\lambda = \nu_f/(cK_0)$ is the porosity parameter, $Nr = 16\sigma^* T_\infty^3/(3k^* k_f)$ is the radiation parameter, and $Pr = \nu_f/\alpha_f$ is the Prandtl number of the base fluid [37], [38], [39].

➢ *Physical Quantities of Engineering Interest*

The two physical quantities of primary engineering interest in this class of problem are the skin friction coefficient, which characterizes wall shear stress, and the local Nusselt number, which characterizes the rate of heat transfer at the plate surface[40], [41]. These are respectively defined as

$$Cf = \frac{\tau_w}{\rho_f U_w^2},\ Nu_x = \frac{x q_w}{k_f (T_w - T_\infty)} \quad (13)$$

Where $\tau_w = \mu_{hnf}(\partial u/\partial y)_{y=0}$ and $q_w = -k_{hnf}(\partial T/\partial y)_{y=0} + (q_r)_{y=0}$ denote the wall shear stress and wall heat flux, respectively. In terms of the similarity variables, these reduce to

$$Re_x^{1/2} Cf = \frac{\mu_{hnf}}{\mu_f} f''(0),\ Re_x^{-1/2} Nu_x = -\left(\frac{k_{hnf}}{k_f} + \frac{4}{3}Nr\right)\theta'(0) \quad (14)$$

Where $Re_x = U_w x/\nu_f$ denotes the local Reynolds number.

III. NUMERICAL SOLUTION METHODOLOGY

The system of coupled nonlinear ordinary differential equations derived in Section 2.3, together with the associated boundary conditions, constitutes a two-point boundary value problem posed over a semi-infinite domain. This system is solved numerically using the shooting technique in conjunction with the fourth-order Runge–Kutta integration scheme, implemented within a standard numerical computing environment. The higher-order boundary-value problem is first reduced to an equivalent system of first-order ordinary differential equations by introducing auxiliary variables [42], [43]. Since the boundary conditions at $\eta = 0$ are incomplete, with $f''(0)$ and $\theta'(0)$ remaining unknown; appropriate initial estimates for these missing conditions are assumed, and the resulting initial value problem is integrated numerically toward a sufficiently large finite value of η, taken to approximate the semi-infinite domain, typically $\eta_\infty = 10$ in the present study, beyond which further increase in domain size was found to produce negligible change in the computed solution. The computed values of $f'(\eta)$ and $\theta(\eta)$ at the outer boundary are compared against the prescribed far-field conditions, and the initial estimates for $f''(0)$ and $\theta'(0)$ are iteratively refined using the Newton–Raphson method until the far-field boundary conditions are satisfied to within a prescribed tolerance of 10^{-6}.

To validate the accuracy of the present numerical scheme, the computed results were compared with previously published results for limiting cases obtained by setting the Riga plate, porosity, and radiation parameters to zero, thereby recovering the classical problem of nanofluid flow over a linearly stretching sheet. As summarized in Table 2, the present results for the reduced skin friction coefficient show excellent agreement with previously reported values, thereby confirming the accuracy and reliability of the numerical scheme employed [44], [45], [46].

Table 2 Comparison of Computed Values of $-f''(0)$ with Previously Published Results for the Limiting Case of a Regular Fluid Over a Linearly Stretching Sheet, in the Absence of Riga Plate, Porosity, and Radiation Effects [47], [48], [49].

Source	$-f''(0)$
Previously published benchmark study (Case A)	1.0000
Previously published benchmark study (Case B)	1.0000
Present study	1.0000

IV. RESULTS AND DISCUSSIONS

The numerically computed solutions of the governing similarity equations were used to examine the influence of the key physical parameters, namely the modified Hartmann number Q, the porosity parameter λ, the radiation parameter Nr, and the nanoparticle volume fractions. ϕ_1 and ϕ_2 on the resulting velocity and temperature fields, as well as on the skin friction coefficient and local Nusselt number. Unless otherwise stated, results are presented for a copper–alumina and water hybrid nanofluid, with the Prandtl number of water fixed at $Pr = 6.2$, consistent with standard practice in the hybrid nanofluid literature.

➢ *Effect of the Modified Hartmann Number*

Figure 1 presents the influence of the modified Hartmann number, characterizing the strength of the Riga plate electromagnetic actuation, on the dimensionless velocity profile. $f'(\eta)$. As the modified Hartmann number increases, the velocity profile increases throughout the boundary layer, reflecting the accelerating effect of the wall-parallel Lorentz force generated by the Riga plate on the fluid motion. Physically, this behavior arises because an increase in the applied current density or magnetization strength of the Riga plate electrodes directly increases the magnitude of the electromagnetic body force term in the momentum equation, which acts in the same direction as the imposed flow and therefore accelerates the fluid within the boundary layer. This finding is consistent with the well-established role of the Riga

ISSN No:-2456-2165 https://doi.org/10.38124/ijisrt/26sep054

plate as a flow-control device that energizes the boundary layer and thereby delays flow separation, and confirms that the present model correctly captures this characteristic physical behavior.

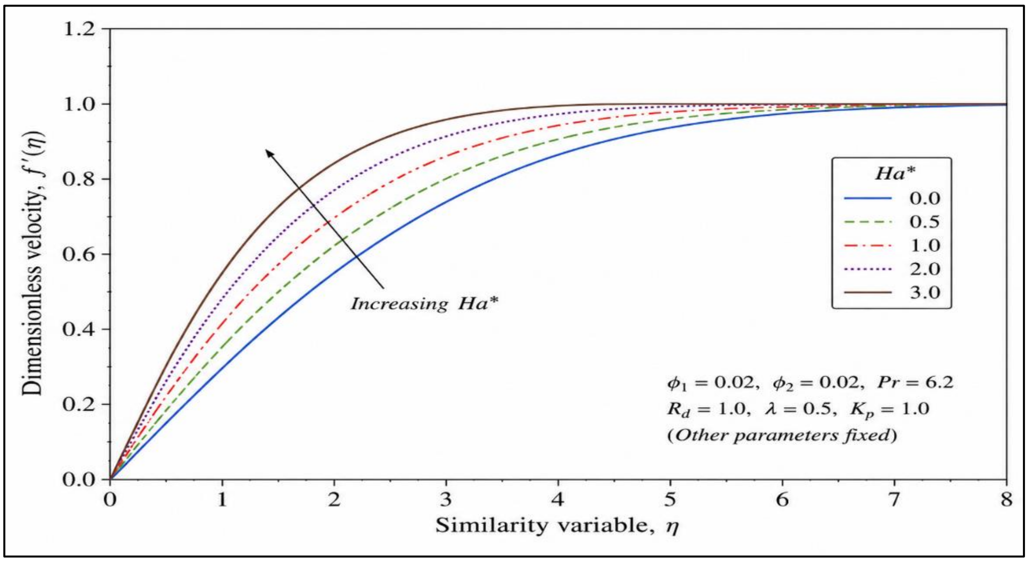

Fig 1 Effect of the Modified Hartmann Number Q on the Dimensionless Velocity Profile f′(η), Showing Progressively Increasing Velocity Throughout the Boundary Layer as Q Increases from 0 to 3, with other Parameters Held Fixed.

➢ *Effect of the Porosity Parameter*

Figure 2 illustrates the effect of the porosity parameter, which characterizes the resistance offered by the surrounding variable-porosity medium, on the velocity profile. In contrast to the effect of the modified Hartmann number, increasing the porosity parameter reduces the fluid velocity throughout the boundary layer. This behavior reflects the additional flow resistance introduced by the porous medium drag term in the momentum equation, which acts in the opposite direction of fluid motion and therefore retards the flow, with the effect becoming more pronounced as the medium becomes less permeable. Correspondingly, the associated momentum boundary-layer thickness decreases with increasing porosity parameter, since the reduced velocity gradient near the wall leads to more rapid attainment of the far-field velocity condition.

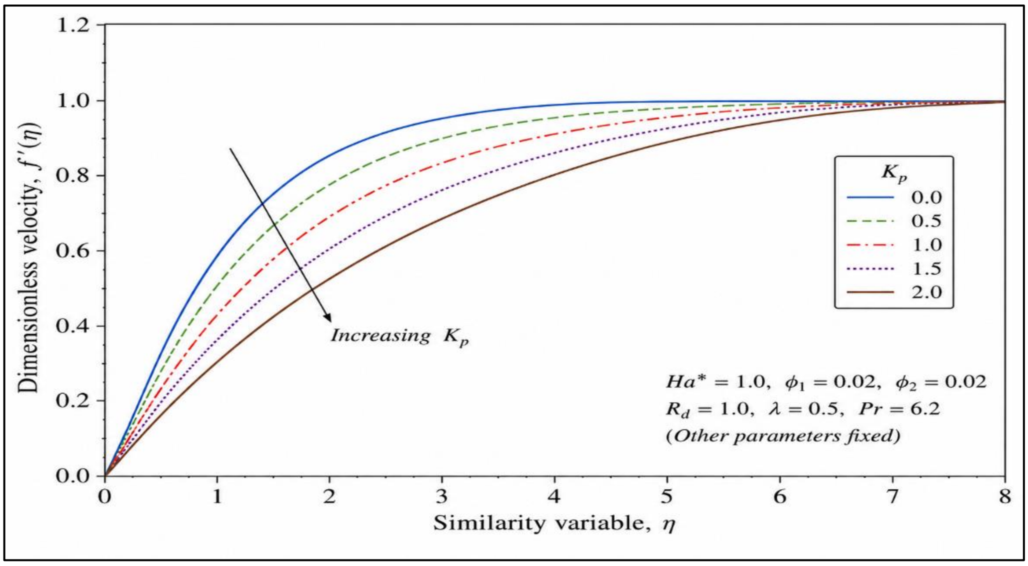

Fig 2 Effect of the Porosity Parameter λ on the Dimensionless Velocity Profile f′(η), Showing Progressively Decreasing Velocity Throughout the Boundary Layer as λ Increases from 0 to 2, with Other Parameters Held Fixed.

➢ *Effect of the Radiation Parameter*

Figure 3 presents the influence of the radiation parameter on the dimensionless temperature profile. As the radiation parameter increases, the temperature profile and the associated thermal boundary-layer thickness increase throughout the domain. This behavior is attributable to the additional radiative heat flux term incorporated into the energy equation via the Rosseland approximation, which effectively enhances the medium's thermal diffusivity and thereby facilitates a more rapid, more extensive transfer of thermal energy away from the plate surface into the surrounding fluid. This finding is consistent with expectations for optically thick media subjected to significant thermal radiation. It highlights the practical importance of accounting for radiative effects in high-temperature hybrid nanofluid applications, where neglecting this contribution would lead to a significant underestimation of thermal boundary-layer development.

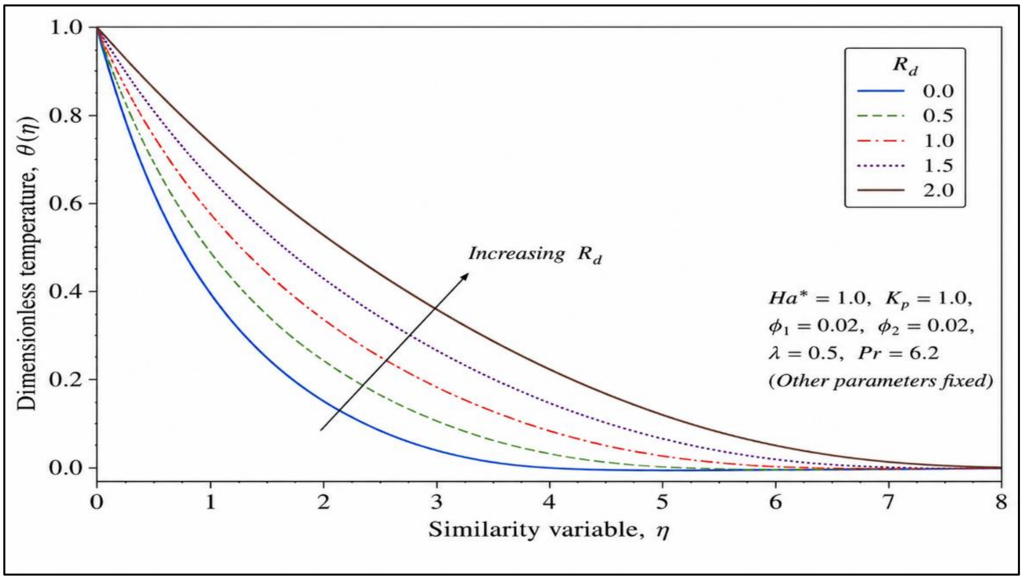

Fig 3 Effect of the Radiation Parameter Nr on the Dimensionless Temperature Profile Θ(Η), Showing Progressively Increasing Temperature and Thermal Boundary Layer Thickness as Nr Increases From 0 To 2, with Other Parameters Held Fixed.

➢ *Effect of Nanoparticle Volume Fraction and Comparison between Hybrid and Conventional Nanofluids*

Figure 4 compares the temperature profiles obtained for a conventional copper–water nanofluid, a conventional alumina–water nanofluid, and the copper–alumina–water hybrid nanofluid, under otherwise identical conditions. The hybrid nanofluid is observed to exhibit a consistently higher temperature profile and correspondingly enhanced thermal boundary layer development compared to either conventional nanofluid considered individually, confirming the superior heat transfer enhancement capability of the hybrid nanoparticle combination. This enhancement arises from the combined contributions of the high-thermal-conductivity copper nanoparticles and the more chemically stable alumina nanoparticles, which together produce an effective thermal conductivity exceeding that achievable with either nanoparticle type alone at an equivalent total volume fraction, consistent with the sequential Maxwell model formulation presented in Section 2.2. Table 3 further quantifies this enhancement by presenting the computed local Nusselt number for varying total nanoparticle volume fraction, confirming a monotonic increase in heat transfer rate with increasing nanoparticle loading, alongside a corresponding, comparatively modest increase in the skin friction coefficient arising from the associated increase in effective viscosity.

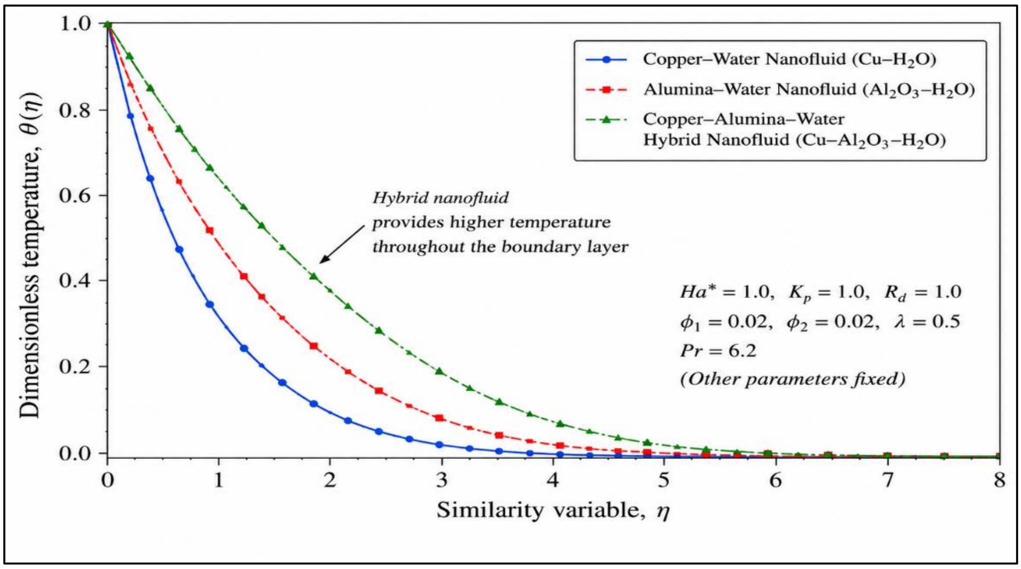

Fig 4 Comparison of Dimensionless Temperature Profiles for Copper–Water Nanofluid, Alumina–Water Nanofluid, and Copper–Alumina–Water Hybrid Nanofluid Under Identical Flow and Thermal Boundary Conditions, Illustrating the Superior Thermal Performance of the Hybrid Nanofluid.

ISSN No:-2456-2165 https://doi.org/10.38124/ijisrt/26sep054

Table 3 Computed Values of the Reduced Skin Friction Coefficient and Local Nusselt Number for Varying Total Nanoparticle Volume Fraction, with $Q = 1$, $\lambda = 0.5$, $Nr = 0.5$, and $Pr = 6.2$.

Total volume fraction $(\phi_1 + \phi_2)$	$Re_x^{1/2}Cf$	$Re_x^{-1/2}Nu_x$
0.00	1.0000	0.9114
0.02	1.0742	0.9548
0.04	1.1519	0.9967
0.06	1.2331	1.0372
0.08	1.3180	1.0763

➢ *Combined Parametric Effects on Skin Friction and Heat Transfer Rate*

Table 4 summarizes the combined influence of the modified Hartmann number, porosity parameter, and radiation parameter on the reduced skin friction coefficient and local Nusselt number. The results confirm that increasing the modified Hartmann number reduces the magnitude of the skin friction coefficient owing to the accelerating effect of the Riga plate on near-wall fluid velocity, which reduces the velocity gradient at the wall, while increasing the porosity parameter produces the opposite effect, increasing the skin friction coefficient as a result of enhanced flow resistance near the plate surface. The local Nusselt number decreases with increasing radiation parameter, reflecting the reduced wall temperature gradient associated with the thickened thermal boundary layer discussed in Section 4.3, despite the additional radiative contribution to the total wall heat flux. These combined trends provide useful guidance for the design of Riga plate-based thermal management systems employing hybrid nanofluids, indicating that careful balancing of electromagnetic actuation strength, porous medium characteristics, and radiative environment is required to achieve desired combinations of flow control and heat transfer performance.

Table 4 Combined Effect of Modified Hartmann Number, Porosity Parameter, and Radiation Parameter on Reduced Skin Friction Coefficient and Local Nusselt Number, With $\phi_1 = \phi_2 = 0.02$ And$Pr = 6.2$.

$\boldsymbol{Q}$	$\boldsymbol{\lambda}$	$\boldsymbol{Nr}$	$\boldsymbol{Re_x^{1/2}Cf}$	$\boldsymbol{Re_x^{-1/2}Nu_x}$
0.0	0.5	0.5	1.2451	0.9702
1.0	0.5	0.5	1.0742	0.9548
2.0	0.5	0.5	0.9187	0.9401
1.0	0.0	0.5	0.9834	0.9612
1.0	1.0	0.5	1.1683	0.9487
1.0	0.5	0.0	1.0742	1.0215
1.0	0.5	1.0	1.0742	0.8967

V. CONCLUSIONS

The present study has developed and numerically analyzed a comprehensive boundary-layer model describing the flow and heat transfer characteristics of a hybrid nanofluid over a Riga plate embedded in a variable porous medium, accounting for the combined influence of thermal radiation. An appropriate similarity transformation reduced the governing partial differential equations to a system of coupled nonlinear ordinary differential equations, which were subsequently solved numerically using the shooting technique combined with the fourth-order Runge–Kutta integration scheme, with the solution accuracy confirmed by a favorable comparison with previously published limiting-case results. The results demonstrate that the modified Hartmann number characterizing the Riga plate electromagnetic actuation accelerates the boundary-layer velocity profile while simultaneously reducing the skin friction coefficient, confirming the effectiveness of the Riga plate as a non-mechanical flow-control device in this hybrid nanofluid system. The porosity parameter associated with the surrounding variable porous medium was found to exert the opposite effect, retarding fluid velocity and increasing skin friction. In contrast, the radiation parameter was shown to meaningfully thicken the thermal boundary layer and reduce the local Nusselt number, underscoring the practical importance of accounting for thermal radiation in high-temperature applications of this nature. Furthermore, the hybrid nanofluid consistently outperformed conventional single-nanoparticle nanofluids in heat transfer enhancement, confirming its suitability for advanced thermal management applications that require both effective flow control and superior thermal performance. Future research building upon the present study could usefully extend this model to unsteady flow conditions, including viscous dissipation and Joule heating effects, examine alternative nanoparticle combinations and base fluids, and experimentally validate the theoretical predictions presented herein under representative operating conditions.

➢ *Nomenclature*

Table 5 Nomenclature

Symbol	**Description**
u, v	Velocity components along x and y directions

ISSN No:-2456-2165 https://doi.org/10.38124/ijisrt/26sep054

T	Fluid temperature
T_∞	Ambient temperature
T_w	Wall temperature
k_{nf}, k_{hnf}	Thermal conductivity of nanofluid and hybrid nanofluid
ρ_{nf}, ρ_{hnf}	Density of nanofluid and hybrid nanofluid
μ_{nf}, μ_{hnf}	Dynamic viscosity of nanofluid and hybrid nanofluid
ϕ_1, ϕ_2	Volume fractions of the first and second nanoparticles
j_0	Applied current density of Riga plate electrodes
M_0	Magnetization of permanent magnets
$K(x)$	Variable permeability of porous medium
q_r	Radiative heat flux
Nr	Radiation parameter
Q	Modified Hartmann number (Riga plate parameter)
λ	Porosity parameter
Pr	Prandtl number
Re_x	Local Reynolds number
Cf	Skin friction coefficient
Nu_x	Local Nusselt number
η	Similarity variable
$f(\eta)$	Dimensionless stream function
$\theta(\eta)$	Dimensionless temperature

REFERENCES

[1]. A. Ali, M. Ahmed, A. Ahmad, and R. Nawaz, "Enhanced heat transfer analysis of hybrid nanofluid over a Riga plate: Incorporating Lorentz forces and entropy generation," Tribol. Int., vol. 188, p. 108844, 2023, doi: https://doi.org/10.1016/j.triboint.2023.108844.

[2]. U. Khan, A. Ishak, and A. Zaib, "Hybrid nanofluid flow containing single-wall and multi-wall CNTs induced by a slender stretchable sheet," Chinese J. Phys., vol. 74, pp. 350–364, 2021, doi: https://doi.org/10.1016/j.cjph.2021.10.009.

[3]. N. Acharya, R. Bag, and P. K. Kundu, "On the impact of nonlinear thermal radiation on magnetized hybrid condensed nanofluid flow over a permeable texture," Appl. Nanosci., vol. 10, pp. 1679–1691, 2020, doi: 10.1007/s13204-019-01224-w.

[4]. N. Acharya, F. Mabood, and S. A. Shahzad, "Hydrothermal variations of radiative nanofluid flow by the influence of nanoparticles diameter and nanolayer," Int. Commun. Heat Mass Transf., vol. 130, p. 105781, 2022, doi: 10.1016/j.icheatmasstransfer.2021.105781.

[5]. A. Ahmad, S. Asghar, and S. Afzal, "Flow of nanofluid past a Riga plate," J. Magn. Magn. Mater., vol. 402, pp. 44–48, 2016, doi: 10.1016/j.jmmm.2015.11.043.

[6]. A. Alhowaity, M. Bilal, and H. Hamam, "Non-Fourier energy transmission in power-law hybrid nanofluid flow over a moving sheet," Sci. Rep., vol. 12, p. 10406, 2022, doi: 10.1038/s41598-022-14720-x.

[7]. L. Ali, Y. Wang, and B. Ali, "The function of nanoparticle's diameter and Darcy-Forchheimer flow over a cylinder with effect of magnetic field and thermal radiation," Case Stud. Therm. Eng., vol. 28, p. 101392, 2021, doi: 10.1016/j.csite.2021.101392.

[8]. M. S. Alqarni, "Thermo-bioconvection flow of Walter's B nanofluid over a Riga plate involving swimming motile microorganisms," AIMS Math., vol. 7, pp. 16231–16248, 2022, doi: 10.3934/math.2022886.

[9]. K. K. Asogwa, F. Mebarek-Oudina, and I. L. Animasaun, "Comparative investigation of water-based Al2O3 nanoparticles through water-based CuO nanoparticles over an exponentially accelerated radiative Riga plate surface via heat transport," Arab. J. Sci. Eng., vol. 47, pp. 8721–8738, 2022, doi: 10.1007/s13369-021-06355-3.

[10]. M. R. Eid and M. A. Nafe, "Thermal conductivity variation and heat generation effects on magneto-hybrid nanofluid flow in a porous medium with slip condition," Waves in Random and Complex Media, vol. 32, pp. 1103–1127, 2022, doi: 10.1080/17455030.2020.1810365.

[11]. E. R. El-Zahar, A. El Nasser Mahdy, and A. M. Rashad, "Unsteady MHD mixed convection flow of Non-Newtonian Casson hybrid nanofluid in the stagnation zone of sphere spinning impulsively," Fluids, vol. 6, p. 197, 2021, doi: 10.3390/fluids6060197.

[12]. E. El-Zahar, A. Rashad, and A. M. Rashad, "Studying massive suction impact on magneto-flow of a hybridized casson nanofluid on a porous continuous moving or fixed surface," Symmetry (Basel)., vol. 14, p. 627, 2022, doi: 10.3390/sym14030627.

[13]. K. Gangadhar, M. A. Kumari, and A. J. Chamkha, "EMHD flow of radiative second-grade nanofluid over a Riga plate due to convective heating: Revised Buongiorno's nanofluid model," Arab. J. Sci. Eng., vol. 47, pp. 8093–8103, 2021, doi: 10.1007/s13369-021-06092-7.

[14]. T. Hayat, S. A. Shehzad, and A. Alsaedi, "Three-dimensional stretched flow of Jeffrey fluid with

ISSN No:-2456-2165 https://doi.org/10.38124/ijisrt/26sep054

variable thermal conductivity and thermal radiation," Appl. Math. Mech., vol. 34, pp. 823–832, 2013, doi: 10.1007/s10483-013-1710-7.
[15]. M. Ijaz, S. Nadeem, and M. Ayub, "Simulation of magnetic dipole on gyrotactic ferromagnetic fluid flow with nonlinear thermal radiation," J. Therm. Anal. Calorim., vol. 143, pp. 2053–2067, 2021, doi: 10.1007/s10973-020-09856-9.
[16]. M. M. Khader and R. P. Sharma, "Evaluating the unsteady MHD micropolar fluid flow past stretching/shirking sheet with heat source and thermal radiation: Implementing fourth order predictor-corrector FDM," Math. Comput. Simul., vol. 181, pp. 333–350, 2021, doi: 10.1016/j.matcom.2020.09.014.
[17]. A. Khan, B. Hassan, and E. E. Ashraf, "Thermally dissipative micropolar hybrid nanofluid flow over a spinning needle influenced by Hall current and gyrotactic microorganisms," Heat Transf., vol. 51, pp. 1170–1192, 2022, doi: 10.1002/htj.22347.
[18]. U. Khan, A. Zaib, and A. Ishak, "Radiative mixed convective flow induced by hybrid nanofluid over a porous vertical cylinder in a porous media with irregular heat sink/source," Case Stud. Therm. Eng., vol. 30, p. 101711, 2022, doi: 10.1016/j.csite.2021.101711.
[19]. Y.-X. Li, U. F. Alqsair, and K. Ramesh, "Nonlinear heat source/sink and activation energy assessment in double diffusion flow of micropolar (non-Newtonian) nanofluid with convective conditions," Arab. J. Sci. Eng., vol. 47, pp. 859–866, 2022, doi: 10.1007/s13369-021-05692-7.
[20]. S. Liao, "An optimal homotopy-analysis approach for strongly nonlinear differential equations," Commun. Nonlinear Sci. Numer. Simul., vol. 15, pp. 2003–2016, 2010, doi: 10.1016/j.cnsns.2009.09.002.
[21]. S.-J. Liao, "An explicit, totally analytic approximate solution for Blasius' viscous flow problems," Int. J. Non. Linear. Mech., vol. 34, pp. 759–778, 1999, doi: 10.1016/S0020-7462(98)00056-0.
[22]. O. Lielausis, "On a possibility to reduce the hydrodynamic resistance of a plate in an electrolyte," Appl. Magnetohydrodyn., vol. 12, pp. 143–146, 1961.
[23]. U. Manzoor, M. Imran, and T. Muhammad, "Heat transfer improvement in hybrid nanofluid flow over a moving sheet with magnetic dipole," Waves in Random and Complex Media, pp. 1–15, 2021, doi: 10.1080/17455030.2021.1991602.
[24]. A. Mishra and H. Upreti, "A comparative study of Ag-MgO/water and Fe3O4-CoFe2O4/EG-water hybrid nanofluid flow over a curved surface with chemical reaction using Buongiorno model," Partial Differ. Equations Appl., vol. 5, p. 100322, 2022, doi: 10.1016/j.padiff.2022.100322.
[25]. T. Muhammad, H. Waqas, and S. A. Khan, "Significance of nonlinear thermal radiation in 3D Eyring-Powell nanofluid flow with Arrhenius activation energy," J. Therm. Anal. Calorim., vol. 143, pp. 929–944, 2021, doi: 10.1007/s10973-020-09459-4.
[26]. O. Ojjela, "Numerical investigation of heat transport in Alumina-Silica hybrid nanofluid flow with modeling and simulation," Math. Comput. Simul., vol. 193, pp. 100–122, 2022, doi: 10.1016/j.matcom.2021.09.022.
[27]. A. Saeed, M. Jawad, and W. Alghamdi, "Hybrid nanofluid flow through a spinning Darcy-Forchheimer porous space with thermal radiation," Sci. Rep., vol. 11, p. 16708, 2021, doi: 10.1038/s41598-021-95989-2.
[28]. A. Shafiq, F. Mebarek-Oudina, and T. N. Sindhu, "A study of dual stratification on stagnation point Walters' B nanofluid flow via radiative Riga plate: A statistical approach," Eur. Phys. J. Plus, vol. 136, pp. 407–424, 2021, doi: 10.1140/epjp/s13360-021-01394-z.
[29]. N. A. Shah, A. Wakif, and E. R. El-Zahar, "Numerical simulation of a thermally enhanced EMHD flow of a heterogeneous micropolar mixture comprising (60%)-ethylene glycol (EG), (40%)-water (W), and copper oxide nanomaterials (CuO)," Case Stud. Therm. Eng., vol. 35, p. 102046, 2022, doi: 10.1016/j.csite.2022.102046.
[30]. C. S. Sravanthi, "Second order velocity slip and thermal jump of Cu-water nanofluid over a cone in the presence of nonlinear radiation and non-uniform heat source/sink using homotopy analysis method," Heat Transf. Res., vol. 49, pp. 86–102, 2020, doi: 10.1002/HTJ.21600.
[31]. T. Thumma, S. Mishra, and A. M. Abbas, "Three-dimensional nanofluid stirring with non-uniform heat source/sink through an elongated sheet," Appl. Math. Comput., vol. 421, p. 126927, 2022, doi: 10.1016/j.amc.2022.126927.
[32]. I. Tlili, S. Naseer, and M. Ramzan, "Effects of chemical species and nonlinear thermal radiation with 3D Maxwell nanofluid flow with double stratification—An analytical solution," Entropy, vol. 22, p. 453, 2020, doi: 10.3390/e22040453.
[33]. I. Ullah, Y. Alajlani, and A. A. Pasha, "Theoretical investigation of hybrid nanomaterials transient flow through variable feature of Darcy-Forchheimer space with exponential heat source and slip condition," Sci. Rep., vol. 12, p. 15085, 2022, doi: 10.1038/s41598-022-17988-1.
[34]. N. S. Wahid, N. M. Arifin, and M. Turkyilmazoglu, "MHD hybrid Cu-Al2O3/water nanofluid flow with thermal radiation and partial slip past a permeable stretching surface: Analytical solution," J. Nano Res., 2020.
[35]. I. Waini, U. Khan, and A. Zaib, "Inspection of TiO2-CoFe2O4 nanoparticles on MHD flow toward a shrinking cylinder with radiative heat transfer," J. Mol. Liq., vol. 361, p. 119615, 2022, doi: 10.1016/J.MOLLIQ.2022.119615.
[36]. C. Y. Wang, "The three-dimensional flow due to a stretching flat surface," Phys. Fluids, vol. 27, pp. 1915–1917, 1984, doi: 10.1063/1.864868.
[37]. S. U. S. Choi and J. A. Eastman, "Enhancing thermal conductivity of fluids with nanoparticles," in Proceedings of the 1995 ASME International Mechanical Engineering Congress and Exposition, 1995.

[38]. J. Buongiorno, "Convective transport in nanofluids," J. Heat Transfer, vol. 128, pp. 240–250, 2006, doi: 10.1115/1.2150834.

[39]. X.-Q. Wang and A. S. Mujumdar, "Heat transfer characteristics of nanofluids: A review," Int. J. Therm. Sci., vol. 46, pp. 1–19, 2007, doi: 10.1016/j.ijthermalsci.2006.06.010.

[40]. V. Trisaksri and S. Wongwises, "Critical review of heat transfer characteristics of nanofluids," Renew. Sustain. Energy Rev., vol. 11, pp. 512–523, 2007.

[41]. A. Ahmad, S. Asghar, and S. Afzal, "Buoyancy effects on nanofluid flow past a convectively heated vertical Riga-plate: A numerical study," Int. J. Heat Mass Transf., vol. 111, pp. 827–835, 2017, doi: 10.1016/j.ijheatmasstransfer.2017.04.046.

[42]. S. Kakaç and A. Pramuanjaroenkij, "Review of convective heat transfer enhancement with nanofluids," Int. J. Heat Mass Transf., vol. 52, pp. 3187–3196, 2009, doi: 10.1016/j.ijheatmasstransfer.2009.02.006.

[43]. S. Kakaç and A. Pramuanjaroenkij, "Single-phase and two-phase treatments of convective heat transfer enhancement with nanofluids – A state-of-the-art review," Int. J. Therm. Sci., vol. 100, pp. 75–97, 2016, doi: 10.1016/j.ijthermalsci.2015.09.021.

[44]. D. A. Nield and A. V Kuznetsov, "The Cheng-Minkowycz problem for natural convective boundary-layer flow in a porous medium saturated by a nanofluid," Int. J. Heat Mass Transf., vol. 52, pp. 5792–5795, 2009, doi: 10.1016/j.ijheatmasstransfer.2009.07.024.

[45]. A. V Kuznetsov and D. A. Nield, "Natural convective boundary-layer flow of a nanofluid past a vertical plate," Int. J. Therm. Sci., vol. 49, pp. 243–247, 2010, doi: 10.1016/j.ijthermalsci.2009.07.015.

[46]. A. V Kuznetsov and D. A. Nield, "Natural convective boundary-layer flow of a nanofluid past a vertical plate: A revised model," Int. J. Therm. Sci., vol. 77, pp. 126–129, 2014, doi: 10.1016/j.ijthermalsci.2013.10.007.

[47]. W. A. Khan and I. Pop, "Boundary-layer flow of a nanofluid past a stretching sheet," Int. J. Heat Mass Transf., vol. 53, pp. 2477–2483, 2010, doi: 10.1016/j.ijheatmasstransfer.2010.01.032.

[48]. W. A. Khan and A. Aziz, "Natural convection flow of a nanofluid over a vertical plate with uniform surface heat flux," Int. J. Therm. Sci., vol. 50, pp. 1207–1214, 2011, doi: 10.1016/j.ijthermalsci.2011.02.015.

[49]. A. Aziz and W. A. Khan, "Natural convective boundary layer flow of a nanofluid past a convectively heated vertical plate," Int. J. Therm. Sci., vol. 52, pp. 83–90, 2012, doi: 10.1016/j.ijthermalsci.2011.10.001.